Design of a New Relieving-DC-Saturation Hybrid Reluctance Machine for Fault-Tolerant In-Wheel Direct Drive

Xing Zhao, Shuangxia Niu *IEEE Senior Member,* Xiaodong Zhang, Weinong Fu

***Abstract*—This paper aims to propose a new hybrid reluctance machine equipped with relieving-DC-saturation ability for electric vehicle in-wheel drive. The proposed machine uses integrated AC and DC current excitation to eliminate extra DC field coils for the efficient torque generation. Besides, considering the inherent DC saturation in stator core caused by DC current excitation, slot PMs are artificially introduced to provide reliving-DC-saturation effect and thus boost torque density. Moreover, with a modular magnetic field configuration, the proposed topology exhibits excellent fault-tolerant potential at both open-circuit and short-circuit condition, making it suitable for safety-critical in-wheel vehicle propulsion. In this paper, the machine configuration and operation principle are introduced, with emphasis on its reliving-DC-saturation effect and corresponding design consideration. Further, performance of this new topology is evaluated by both finite element analysis and prototype experiments. It is revealed that, with this relieving-DC-saturation ability, torque density of the proposed machine can be enhanced by about 25% under relatively high current density.**

***Index Terms*—DC saturation effect, hybrid reluctance machine, integrated current excitation, modular magnetic field, slot PMs.**

I. Introduction

With the increasing concern of environmental protection and energy saving, developing electric vehicles (EV) becomes been an important trend over the world [1]. For modern EVs, using in-wheel direct-drive machines to provide propulsion power has been regarded as one important trend, since it owns significant vehicle-level advantages such as improved dynamics index due to fast torque response, enlarged inner space with elimination of mechanical transmission device, and higher efficiency of the whole driving system [2-4]. The traditional permanent magnet (PM) synchronous machine (SPM) has been well established as in-wheel drive due to its high torque density and high efficiency. However, with the limited supply of rare-earth PMs, the cost of SPM increases distinctly. Hence, developing high-performance reluctance machines becomes a hot topic recently [5-6].

Switched reluctance machine (SRM) is a potential non-PM topology for in-wheel direct drive [7-8]. SRM owns a robust mechanical structure. However, its torque performance needs to be improved. On one hand, torque density of SRM is poor than that of traditional PM machines, since SRM can only operate in the first quadrant of BH curve. Some design technique featured by slot PMs has been proposed to extend the BH working range of SRM and boost its torque density [9-11]. On the other hand, torque ripple in SRM is severe caused by half-cycle-conducting principle [12-13], which restricts its practical applications.

Doubly salient machine with DC coils located at stator side, namely DC-DSM, is an emerging non-PM solution. In the early stage, DC-DSM employs distributed DC field excitation and its feasible slot pole combination is similar with that in SRM. With DC coils, air-gap magnetic field is established in DC-DSM [14], which enables DS-DSM to operate in a whole electrical period. However, its torque ripple ratio is still unacceptable due to rich even-order flux harmonics [15]. To address this issue, variable flux reluctance machine (VFRM) is proposed [16]. VFRM uses concentrated DC coils that uniformly wounded on stator teeth. With this change of DC coil layout, the excitation field becomes symmetrical along the air gap and thus more feasible slot pole combinations can be employed in VFRM than that in DC-DSM. Especially, some new slot pole combinations equipped with odd rotor pole pairs are explored [17], in which all even-order flux harmonics are cancelled due to electromagnetic complementary effect. Consequently, compared to DS-DSM, VFRM can obtain smoother toque performance when driven by sinusoidal current [18]. After that, considering the space conflict between AC and DC coils in VFRM, a control strategy is proposed to integrate DC excitation and AC excitation [19]. Specifically, it employs an open-winding drive structure to inject zero-sequence current in armature winding and functions as a virtual DC field source. In this way, the space conflict between AC and DC coils can be eliminated, which further contributes to boosted torque density and efficiency. Meanwhile, with this integrated control method, DC coils can be replaced by DC-biased current at initial design stage. Inspired by this, a variety of new DC-DSM topologies featured by DC-biased current are studied [20-21]. In general, the existing literature of DC-DSM achieves significant progress in terms of the diversity of slot pole combination, even-order harmonics reduction and integrated DC and AC current control. However, a distinct issue, namely DC saturation effect, has not attracted much attention. Specifically, with the use of DC field excitation, the DC-biased magnetization component inevitably exists in stator core, which can't contribute to electromagnetic energy conversion but leads to the increased hysteresis loss and makes the stator core easier to be saturated [22-23].

This paper aims to present a new reluctance machine solution, that can be referred as reliving-DC-saturation hybrid reluctance machine (RDCS-HRM). RDCS-HRM uses integrated AC and DC current excitation and meanwhile eliminates DC saturation effect in the stator core. Consequently, improved torque density is achieved. Moreover, modular magnetic field is constructed in RDCS-HRM, which enables electromagnetic isolation between phases and thus fault-tolerant ability. This paper is organized as follows. In Section II, the machine structure, drive method and operation principle are introduced, with focus on the reliving-DC-saturation principle. Some important design considerations about slot PM dosage and DC current ratio are presented. In Section III, the electromagnetic performance of the proposed machine is evaluated by finite element analysis, considering the influence of RDCS operation on flux distribution, inductance characteristics, torque capacity and power factor. In Section IV, a machine prototype is manufactured and fully tested. Finally, some conclusions are drawn in Section V.

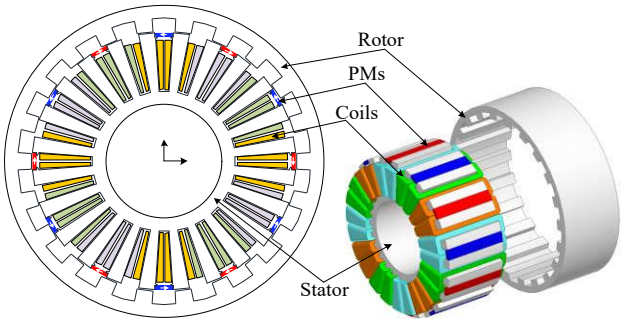

Fig. 1. Configuration of the proposed RDCS-HRM.

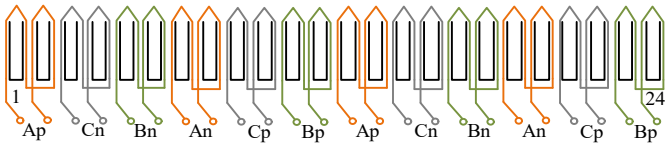

Fig. 2. Winding connection. (P and N refers to polarity distribution)

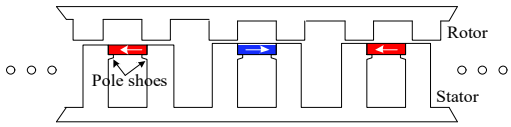

Fig. 3. PM magnetization and arrangement.

II. The Proposed Machine

A. Machine structure

Fig.1 shows the configuration of the proposed RDCS-HRM. This machine employs a 24-slot and 22-pole-pair doubly salient structure. All excitation sources are located at the stator side and the rotor consists of only iron core. The armature winding uses a double-layer concentrated connection as denoted in Fig. 2, in which every two adjacent coils are negatively cascaded together to form an independent sub-phase module. With zero-sequence current injected into the proposed RDCS-HRM, DC current is excited in each sub-phase module, which can function as virtual DC field coils for electromagnetic torque generation. Moreover, considering the inherent biased flux feature of DC field source, slot PMs are artificially introduced to relieve DC saturation in the stator core. As shown in Fig. 3, all slot PMs are magnetized in tangential direction and housed by extra stator pole shoes.

The advantages of the proposed RDCS-HRM are listed as

(1) No excitation components are arranged at rotor side, which ensures a good mechanical robustness.

(2) The application of zero-sequence current control eliminates the requirement of extra DC field coils, thus leading to reduced copper loss and boosted efficiency.

(3) The injection ratio of zero-sequence current can be flexibly controlled, which gives a benefit for flexible torque and speed control to satisfy different EV working conditions.

(4) The introduced PMs on slot openings generates a constant PM flux component at the stator side, which can be utilized to cancel the DC flux component excited by zero-sequence current. Therefore, DC saturation effect in stator core can be mitigated. Consequently, the proposed RDCS-HRM can obtain enhanced torque density with high current density.

(5) Modular magnetic field is constructed, which provides good interphase electromagnetic isolation and fault-tolerant potential. This is important for safety critical EV propulsion.

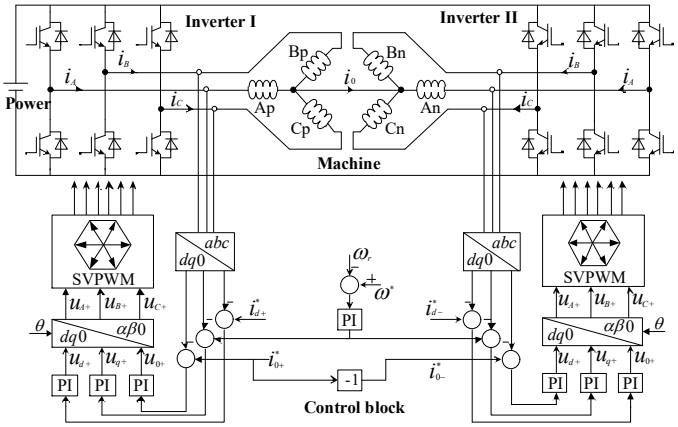

Fig. 4. Drive system for the proposed RDCS-HRM.

B. Drive control method

Fig. 4 shows the drive system for the proposed RDCS-HRM. Sub-phase modules of Ap, Bp, Cp adopts a star connection and fed by an independent inverter. Similarly, Sub-phase modules of An, Bn and Cn are fed by another inverter. The neutral points of two sub-phase groups are linked together to provide a return path for zero-sequence current excitation. To establish modular magnetic field with zero-sequence current excitation, armature current in each module can be written as

$$\begin{cases} i_{\mathrm{Ap}} = i_{ac}\cdot\sin(\theta_e)+i_{dc} \\ i_{\mathrm{Bp}} = i_{ac}\cdot\sin(\theta_e-2\pi/3)+i_{dc} \\ i_{\mathrm{Cp}} = i_{ac}\cdot\sin(\theta_e+2\pi/3)+i_{dc} \\ i_{\mathrm{An}} = i_{ac}\cdot\sin(\theta_e)-i_{dc} \\ i_{\mathrm{Bn}} = i_{ac}\cdot\sin(\theta_e-2\pi/3)-i_{dc} \\ i_{\mathrm{Cn}} = i_{ac}\cdot\sin(\theta_e+2\pi/3)-i_{dc} \end{cases} \tag{1}$$

where i_{Ap}, i_{Bp}, i_{Cp} are the armature current fed by inverter I. i_{An}, i_{Bn}, i_{Cn} are the armature current fed by inverter II. i_{ac} is the AC current component. i_{dc} is the DC current component. θ_e is the rotor electrical angle, which can be further expressed as

$$\theta_e = N_r \frac{d\theta_r}{dt} t + \alpha \tag{2}$$

where N_r is the rotor pole pairs, θ_r is the rotor mechanical angle, t is time, α is the initial electrical angle. Using Clarke and Park transformer matrix, armature current under the ABC coordinate system, can be transformed into $dq0$ coordinate system as

$$\begin{bmatrix} i_d \\ i_q \\ i_0 \end{bmatrix} = \begin{bmatrix} \cos\theta_e & -\sin\theta_e & 0 \\ \sin\theta_e & \cos\theta_e & 0 \\ 0 & 0 & 1 \end{bmatrix} \cdot \sqrt{\frac{2}{3}} \begin{bmatrix} 1 & -\frac{1}{2} & -\frac{1}{2} \\ 0 & \frac{\sqrt{3}}{2} & -\frac{\sqrt{3}}{2} \\ \frac{1}{\sqrt{2}} & \frac{1}{\sqrt{2}} & \frac{1}{\sqrt{2}} \end{bmatrix} \begin{bmatrix} i_A \\ i_B \\ i_C \end{bmatrix} \tag{3}$$

Further, the relationship between zero-sequence current i_0 , and DC current component i_{dc} , can be derived as

$$i_0 = \sqrt{3} i_{dc} \tag{4}$$

It can be found that i_{dc} is proportional to i_0, which means, by controlling i_0 flowing from Inverter I into Inverter II, i_{dc} can be effectively regulated in each sub-phase module.

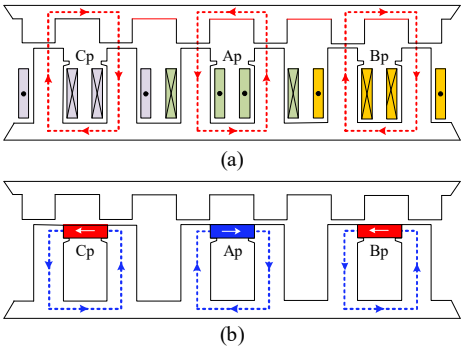

Fig. 5. No-load flux distribution. (a) Only i_{dc}. (b) Only slot PMs.

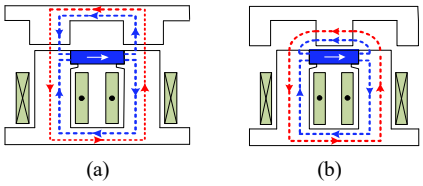

Fig. 6. No-load flux variation of Ap. (a) At *d* axis. (b) At *q* axis.

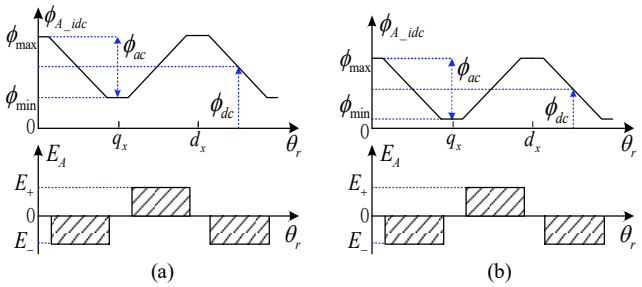

Fig. 7. Schematic flux linkage and back EMF. (a) Only i_{dc}. (b) i_{dc} and PMs.

C. *Relieving-DC-Saturation principle*

Fig. 5 presents the schematic no-load flux distribution under different excitation status. As shown in Fig. 5(a), when only i_{dc} is applied, the flux linkage in each sub-phase module forms an independent magnetic circuit unit. Fig. 5(b) describes the flux distribution with only slot PMs active. It is shown PM flux has a symmetrical modular characteristic as that excited by i_{dc}.

Fig. 6 illustrates the no-load flux variation in each sub-phase module with i_{dc} and slot PMs both active. It can be found that, the flux excited by slot PMs changes its return path when i_{dc} is applied, since part of PM flux is pushed into the air gap, while the other remains at the stator side. It should be pointed out, the boost effect of whole air gap flux is not so distinct, because the flux component excited by i_{dc} in air gap is reduced at the same time due to the existence of slot PM MMF. The main function of slot PMs is reducing stator core saturation by producing an opposite flux bias at the stator side against that excited by i_{dc}, which is referred as relieving-DC-saturation (RDCS) effect in this paper. Specifically, as illustrated in Fig. 7(a), flux generated by i_{dc} is inevitably unipolar due to the existence of DC flux bias excited by average rotor permeance. This DC flux bias makes no contribution to back EMF generation. What's worse, it will increase the saturation level in stator core. However, with the introduction of slot PMs, an opposite PM flux bias is produced at stator side to cancel DC flux bias. In this way, the biased level of flux linkage can be reduced as presented in Fig. 7(b), and the maximum flux density in stator core can be mitigated as well, thus leading to the so-called RDCS effect.

D. *Torque production*

The torque equation of the proposed machine can be derived by differentiating magnetic energy product in each sub-phase module with respect to the rotation movement as

$$T_e = \frac{\delta w_c}{\delta \theta_r} \tag{5}$$

where w_c is the magnetic energy product and can be written as

$$w_c = \frac{1}{2} L_p \left[i_{ac} + i_{dc} \right]^2 \tag{6}$$

where L_p refers to the self-inductance in each sub-phase module. Substituting (6) into (5), the torque equation can be deduced as

$$T_e = \frac{1}{2} i_{dc}^2 \frac{dL_p}{d\theta_r} + \frac{1}{2} i_{ac}^2 \frac{dL_p}{d\theta_r} + i_{dc} i_{ac} \frac{dL_p}{d\theta_r} \tag{7}$$

It can be found the torque of each module has three components. The first term refers to the cogging torque excited by i_{dc} only. The second term refers to the reluctance torque produced by i_{ac} only. The third term refers to the electromagnetic torque excited by the interaction between i_{ac} and i_{dc}. As is well known in SRM, to produce effective reluctance torque, the phase current should be applied in the inductance-rising region and then decreases to zero in the inductance-declining region to avoid negative torque, which means the phase current can only be applied during half of the electrical period. However, in the proposed machine, the phase current is applied in the full electrical period. Therefore, the reluctance torque cannot be utilized but lead to torque ripple. It is the electromagnetic torque excited by i_{ac} and i_{dc} interaction that contributes to average torque in the proposed machine.

E. *Slot pole combination*

In the proposed machine, by selecting slot pole combination, the torque ripple arising from reluctance torque can be reduced. The feasible slot pole combination can be expressed as

$$\begin{cases} N_s = 2mj, \; j = 1, 2, 3 \ldots \\ N_r = N_s \pm 2k, \; k = 1, 2, 3 \ldots \end{cases} \tag{8}$$

where N_s is the number of stator slots. m is the phase number. The cases with odd rotor pole pairs are not adopted considering the unbalanced magnetic pull. The slot angle in the proposed machine can be expressed as

$$\gamma = \frac{360^\circ N_r}{N_s} \tag{9}$$

Then, the electrical angle difference $\Delta\theta_e$ between two adjacent sub-phase modules can be expressed as

$$\Delta\theta_e = (2m\gamma) \bmod (360^\circ) \tag{10}$$

In the proposed design, with the use of 24 stator slots, four cases with 20, 22, 26, 28 rotor pole pairs are considered respectively. Corresponding $\Delta\theta_e$ can be calculated as

$$\Delta\theta_e = \begin{cases} 0^\circ, \; \mathrm{N_r} = 20 \text{ or } 28 \\ 180^\circ, \; \mathrm{N_r} = 22 \text{ or } 26 \end{cases} \tag{11}$$

The rotor pole pairs of 22 and 26 are recommend, because the reluctance torque generated in two adjacent sub-phase modules are opposite and can be cancelled with each other, which means the torque ripple due to reluctance torque can be minimized.

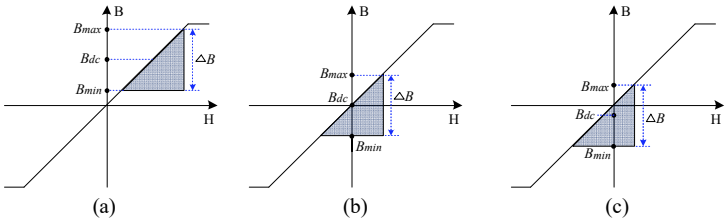

Fig. 8. With PMs increasing. (a) Weak RDCS. (b) Full RDCS. (c) Over RDCS.

F. Design consideration

The influence of slot PM dosage is multidimensional in the proposed RDCS-HRM, which can be illustrated as follows.
(1) With slot PMs increasing, three typical BH curves of stator core are denoted in Fig. 8, in which the DC flux density changes from the positive value to zero and then negative value. The DC flux density is disadvantageous regardless if its polarity. Hence, slot PM cannot be overused to avoid negative DC flux density.
(2) The increase of slot PM dosage leads to the reduction of slot area for electrical load, which may decrease torque density.
(3) PMs bring distinct cost burden, thus cannot be overused.

Therefore, the accurate design of slot PM dosage is the key in the proposed design to obtain a balance between RDCS effect, electrical load reduction and machine cost increase.

The DC current ratio is another important design parameter, which can be defined as

$$k_{dc}=\frac{i_{dc}}{\sqrt{i_{dc}^2+i_{ac}^2}},\ i_{dc}^2+i_{ac}^2\le i_{rms}^2 \tag{12}$$

Where i_{rms} refers to the inverter current scale.
(1) The DC current ratio determines the distribution of magnetic load and electrical load, which affects torque and power factor.
(2) The DC current ratio determines the bias of BH curve and corresponding slot PM dosage needed for optimal RDCS effect.

Based on the above discussion, it is shown design parameters of slot PM dosage and DC current ratio have leading influence on machine performance and they are correlated with each other, which should be carefully evaluated during design stage.

TABLE I
Design Parameters for the Proposed RDCS-HRM

Symbol	Parameter	Unit	Value
d_{ro}	Outer diameter of rotor	mm	150
d_{ri}	Inner diameter of rotor	mm	130
d_{so}	Outer diameter of stator	mm	129
d_{si}	Inner diameter of stator	mm	60
h_{ry}	Height of rotor yoke	mm	5
h_{sy}	Height of stator yoke	mm	5
h_{pm}	Height of slot PMs	mm	Variable
δ	Air gap length	mm	0.5
l	Stack length	mm	80
θ_s	Arc of stator teeth	°	7
θ_r	Arc of rotor salient pole	°	7
	Turns of each coil	-	Variable
	Wire size (AWG)	-	30
	Slot factor	-	0.75
	Current density	A/mm^2	12

TABLE II
Major Materials and Specifications

PMs		Steels	
Material	NdFeB35	Material	MG19_24
Remanence	1.2 T	Saturated point	1.8 T
Coercive force	915 kA/m	Mass density	7650 kg/m^3

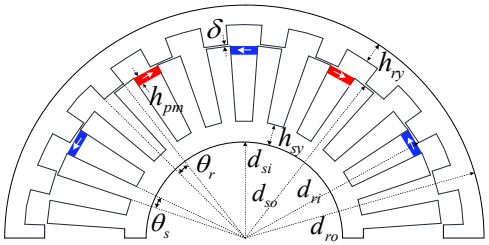

Fig. 9. General dimension parameters.

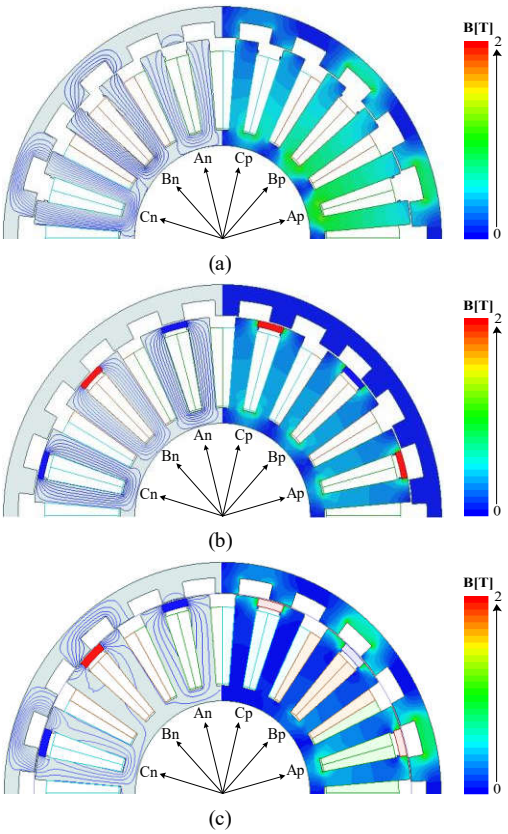

Fig. 10. No-load magnetic field. (a) i_{dc} only. (b) PMs only. (c) i_{dc} and PMs.

III. Electromagnetic Performance

With the commercial software Maxwell, finite element (FE) simulation is performed to assess electromagnetic performance of the proposed topology. Some general dimension parameters are labeled in Fig. 9, with their design values listed in Table I. The major materials and specifications are given in Table II.

A. No-load magnetic field distribution

The no-load magnetic field distribution is plotted in Fig. 10. It can be found that every two stator teeth and rotor salient poles constitute an individual magnetic circuit unit. This modular flux characteristic gives a good interphase electromagnetic isolation and corresponding fault-tolerant potential. Moreover, with the assistance of slot PMs, the flux density of stator core is reduced, while that of rotor core is almost unchanged, which is due to the mitigation of DC flux component in the stator core. The no-load flux linkage with 3A DC current is calculated and presented in Fig. 11. With slot factor fixed at 0.75, different combinations of slot PM dosage and coil turn number are evaluated. When PM height is 3mm and coil turn number is 58, best RDCS effect is achieved with the DC flux component in close to zero.

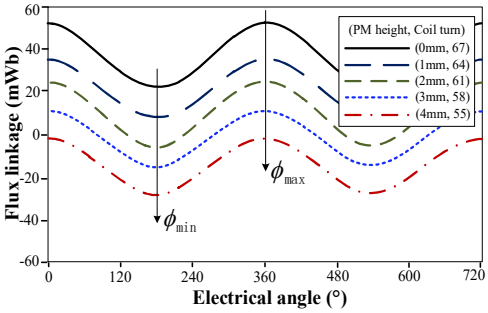

Fig. 11. Flux linkage variation with different slot PM dosage.

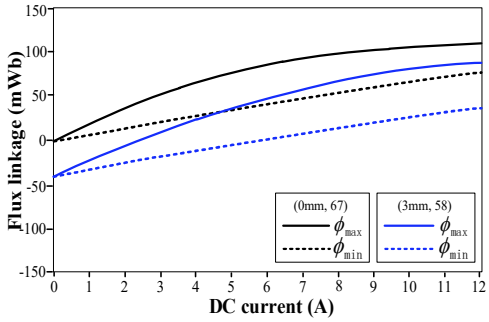

Fig. 12. Maximum and minimum flux contour lines with different i_{dc}.

Further, with different DC current applied, the contour lines of the maximum and minimum values of coil flux linkage are collected and plotted in Fig. 12. It can be seen, with the increase of DC current, the maximum value of coil flux linkage tends to be saturated, while the minimum value keeps growing linearly. However, with the assistance of slot PMs, the saturation trend of the maximum coil flux linkage can be slowed down, and thus broadened difference between the maximum and minimum coil flux values can be achieved for boosted electromagnetic energy conversion, especially with large DC current applied.

B. Torque components analysis

Fig. 13 shows the inductance characteristic of the proposed machine. Benefiting from modular magnetic field distribution, little mutual inductance exists between phases. However, with the rotor rotation, the variation of self-inductance is significant, similar with that in SRMs. As revealed in Equ. (7), three torque components are proportional to the variation of self inductance, which are cogging torque with respect to i_{dc}^2 , reluctance torque with respect to i_{ac}^2, and electromagnetic torque associated with $i_{ac}i_{dc}$, respectively. Obviously, the polarity of armature current has no influence on the cogging torque and reluctance torque due to square relationship. Fig. 14 shows the integrated current excitation, in which DC current and AC current share the same effective value of 3A. The corresponding torque components are calculated and plotted in Fig. 15(a). It can be seen, distinct reluctance torque is generated, which is bipolar and alternating, thus cannot produce effective average torque but leads to severe torque ripple. In this paper, the slot pole design of the proposed topology is artificially selected as 24-slot and 22-pole-pair to construct electromagnetic complementation between every two adjacent sub-phase modules. As shown in Fig. 15(a), the phase angles of reluctance torque in two sub-phase modules have 180° difference and thus can be cancelled. Consequently, as shown in Fig. 15(b), smooth steady torque with only 7% torque ripple ratio can be achieved in the proposed machine.

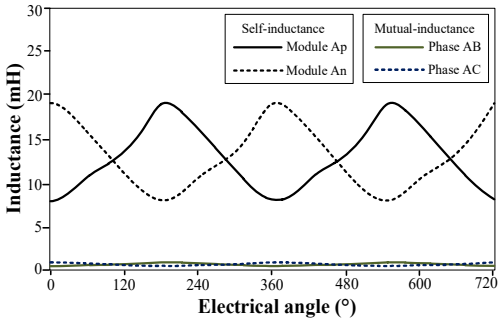

Fig. 13. Self inductance and mutual inductance.

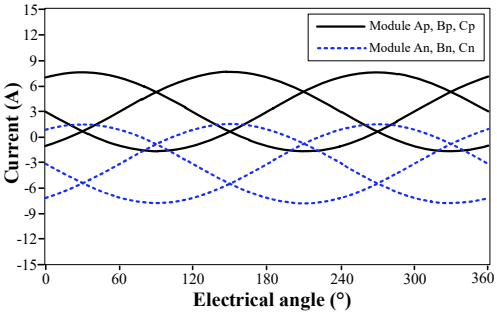

Fig. 14. Integrated AC and DC current excitation.

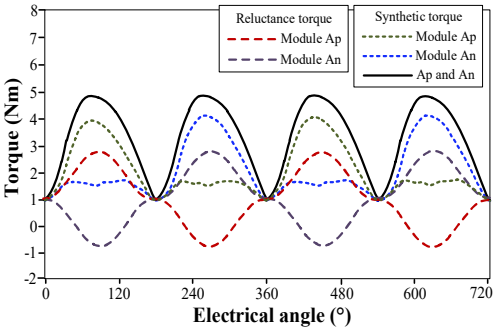

(a)

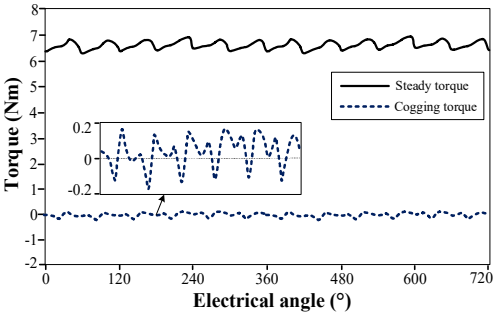

(b)

Fig. 15. (a) Torque component analysis. (b) Steady torque performance

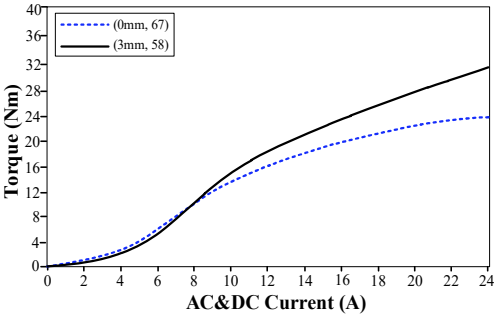

Fig. 16. Torque capacity with and without RDCS effect.

C. Torque capacity

Fig. 16 presents the torque capacity of the proposed machine. The AC and DC current share the same effective value with the change of whole current excitation. When current excitation is less than 9A, the output torque with slot PMs is a little smaller than that without slot PMs. This is because at this condition, the stator core is not saturated, and introduction of slot PMs brings electrical load reduction. When current excitation is larger than 9A, the output torque with slot PMs is obviously higher due to DC saturation reduction. In general, if the cooling condition is allowed, introduction of slot PMs can increase torque density by 25% with relatively large current excitation.

TABLE III
Power, Loss and Efficiency at the Rated Condition

	Without RDCS	With RDCS
Rated power (W)	1675	1937
Copper loss (W)	388	337
Core loss (W)	78	70
PM eddy current loss (W)	-	14
Efficiency (%)	78%	82%

D. Loss, efficiency and heat

The loss and efficiency of the proposed machine at the rated condition are examined. Relevant data are listed in Table III. It is shown, with the RDCS operation, higher rated power can be achieved, and less copper loss is consumed with the reduction of coil turn number. The core loss and PM eddy current loss are much less than the copper loss due to low-speed characteristic. Consequently, with the RDCS operation, the rated efficiency is improved. Moreover, since the total loss is reduced from 466W to 421W, the heat issue of stator can be also relieved.

E. Influence of DC current ratio

Fig. 17 shows the influence of different DC current injection on the output torque performance. The whole current excitation is set at 12A to examine the influence of stator saturation effect. It is shown that regardless of the slot PM dosage, the maximum torque always arrives at the point with 50% DC current applied. This is because, at this point, the electrical load and magnetic load are balanced and thus co-energy is maximized.

Power factor (PF) is one of the leading influence parameters on the inverter scale. In this paper, the ratio of active power to apparent power of the phase winding is employed to assess PF. The calculated PF with different DC current ratio is shown in Fig. 18. It reveals, the larger DC current ratio is, the better PF is obtained. Besides, with the RDCS operation, PF is improved to some extent. This can be explained by the PF equation as

$$PF = \frac{1}{\sqrt{1+(\frac{X_q I_q}{E_0})^2}} \tag{13}$$

where E_0 is the phase back EMF. X_q is the q-axis inductance. I_q is the q-axis current. With the assistance of slot PMs, saturation effect in stator core can be effectively mitigated. Consequently, a larger variation range of no-load flux linkage and phase back EMF E_0 can be achieved with reduced electrical load, which contributes to improved PF performance.

In general, to obtain acceptable torque density and PF both, the injection ratio of DC field current in the proposed topology is recommended to be equal to or larger than 0.5.

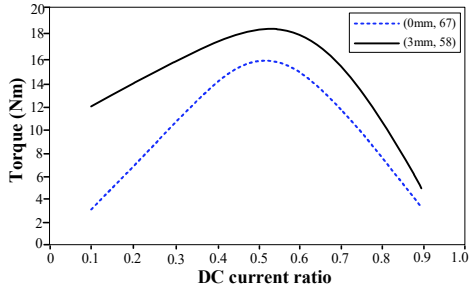

Fig. 17. Influence of DC current ratio on torque capacity.

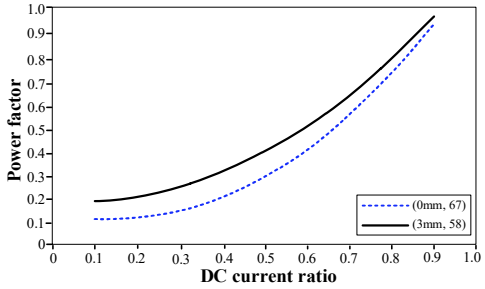

Fig. 18. Influence of DC current ratio on power factor

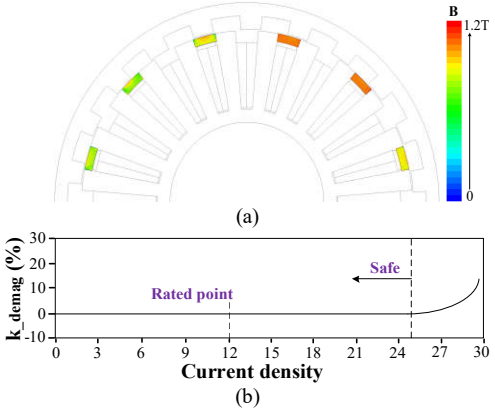

Fig. 19. (a) Flux density distribution. (b) PM demagnetization ratio.

F. PM demagnetization

The PM demagnetization risk is influenced by both armature magnetomotive force (MMF) and environmental temperature, considering the no-linear B–H characteristics of PMs. To check the PM demagnetization behavior in the proposed topology, the total loss at the rated condition is calculated, which is involved in the co-simulation iteration between electromagnetic field and temperature field. In this way, the environmental temperature and relevant B-H characteristic of PMs under this temperature can be determined for demagnetization evaluation. For NdFeB magnet, the knee point of irreversible demagnetization is 0.33T at 125°. Fig. 19(a) shows the flux density distribution of PMs at the rated condition. The minimum flux density of PMs is 0.65T, thus no demagnetization exists. For a quantitative evaluation, the PM demagnetization ratio is further defined as

$$k_{demag} = \frac{E_1 - E_2}{E_1} \times 100\% \tag{14}$$

where E_1 and E_2 are back-EMF fundamental amplitudes before and after applying current excitation, respectively. As shown in Fig. 19(b), when the current density is less than 25A/mm^2, the demagnetization ratio keeps at zero, thus PMs are safe.

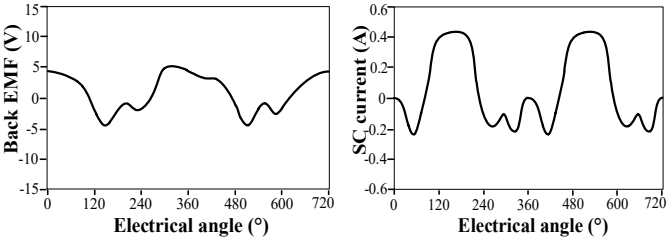

(a) (b)

Fig. 20. Fault performance (a) Open circuit voltage. (b) Short circuit current

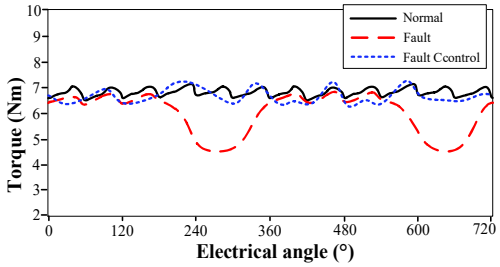

Fig. 21. Torque performance at normal, fault and fault control conditions.

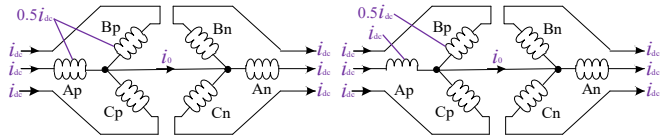

(a) (b)

Fig. 22. Illustration of DC current distribution. (a) Normal. (b) Open circuit.

IV. Fault Tolerant Performance

The traditional PM machines perform well for EV propulsion. However, under fault conditions, they still face some challenges. Specially, large induced voltage usually exists in traditional PM machines if open circuit fault happens, which could breakdown power devices. What's worse, if short circuit fault occurs, large interturn current may emerge and make machine overheated.

In the proposed RDCS-HRM, benefiting from the modular magnetic field distribution, a good electromagnetic isolation is achieved between phases. The open circuit voltage of sub-phase Ap at rated condition is calculated and presented in Fig. 20(a). When the machine speed is 1000 rpm, the open circuit voltage of Ap is less than 5V. This is because, on one side, the change of slot PM working point is not distinct with rotor rotation, thus the PM induced voltage can be ignored. On the other side, little mutual-inductance voltage exists with modular magnetic circuit. Fig. 20(b) presents the short-circuit current of Ap at 1000 rpm. The short-circuit current is less than 0.5A. This is due to small open-circuit voltage and relatively large self-inductance.

Fig. 21 shows the calculated torque at normal, fault and fault control conditions. It can be seen, when the open circuit or short circuit occurs in any module, the average torque is reduced, and the torque ripple increases distinctly. However, in the proposed machine, active fault-tolerant control can be realized for torque compensation. Fig. 22 illustrates the DC current distribution at different conditions. It is shown that, at the fault condition, the DC current of the remaining healthy module is actively doubled under the same zero-sequence current control, thus the average electromagnetic torque of the remaining healthy module can be doubled according to Equ. (7). Therefore, the torque reduction at fault condition can be compensated effectively.

TABLE IV
Rated Performance of Three Machines

Parameters	SRM	Proposed	SPM
Outer diameter (mm)	150	150	150
Stack length (mm)	80	80	80
Air gap length (mm)	0.5	0.5	0.5
Stator slot number	24	24	24
Rotor pole pairs	22	22	10
PM volume (mm^3)	-	25200	48500
Current density (A/mm^2)	12	12	12
Torque (Nm)	16.2	18.3	26.8
Cogging torque (Nm)	-	0.05	1.2
Torque ripple ratio (%)	26%	7%	18%
Efficiency (%)	81%	82%	89%
Power factor	0.39	0.47	0.78
Flux weakening ability	Good	Good	Poor
PM demagnetization	-	Safe	Easy
Fault tolerance	Good	Good	Poor

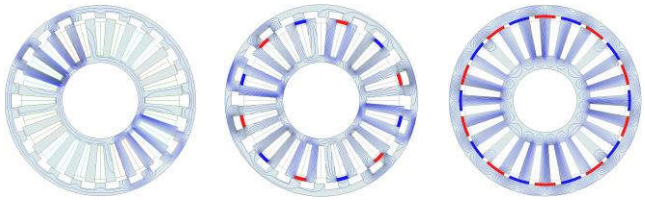

(a) (b) (c)

Fig. 23. On-load flux distribution of three machines. (a) Traditional 24/22 SRM. (b) Proposed 24/22 RDCS-HRM. (c) Traditional 24/20 SPM.

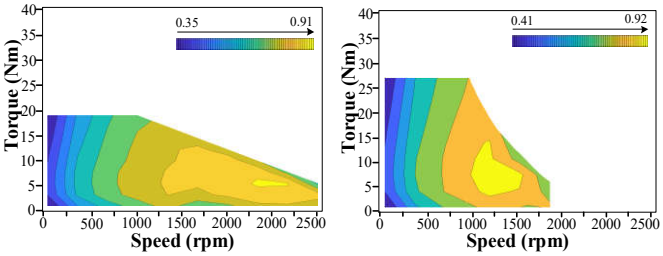

(a) (b)

Fig. 24. Efficiency map. (a) Proposed RDCS-HRM. (c) Traditional SPM.

V. Comparative Study

To examine its usefulness, a comparative study is performed between the proposed RDCS-HRM, the conventional switched reluctance machine (SRM) and surface-mounted PM machine (SPM), which are two well-established candidates for in-wheel EV drive. For a fair comparison, three machines share the same dimension and stack length, air gap length and current density. Fig. 23 shows the on-load flux distribution of three machines. The SRM uses 180° conduction angle control, while the SPM adopts traditional maximum torque per ampere vector control. The comparison results are presented in Table IV. It is shown, compared to SRM, the proposed machine can achieve relatively higher torque density, lower torque ripple ratio as well as higher power factor due to the reduction of armature current harmonics. Compared to SPM, the proposed RDCS-HRM has relatively lower torque density and efficiency. However, RDCS-HRM has lower torque ripple benefiting from neglectable cogging torque, reduced PM demagnetization risk, better fault-tolerance ability and extended torque speed range as shown in Fig. 24, in which the DC bus voltage is set 80V and the maximum effective value of phase current is set 12A during flux weakening.

(a) (b) (c)

Fig. 25. Prototype. (a) Stator. (b) Stator details. (c) Rotor.

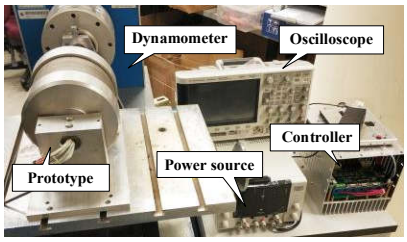

Fig. 26. Test platform for the proposed RDCS-HRM.

TABLE V
Comparison of Prototype and Simulation Performance

	Prototype	RDCS model	Non-RDCS model
Rated speed (rpm)	1000	1000	1000
Rated voltage (V)	36	38	42
Rated torque (Nm)	17.8	18.5	15.9
Rated Power (W)	1863	1937	1675
Copper loss	345	337	388
Efficiency	81%	82%	78%

VI. Experimental Verification

To demonstrate the feasibility of the proposed RDCS-HRM, a prototype is manufactured. Relevant dimensions are in line with the design values listed in Table I. The PM height is 3mm and the coil turn number is 58. Fig. 25 shows the manufacturing details of the prototype. Fig. 25(a) and Fig. 25(b) show the stator assembly. Extra pole shoes are designed with stator teeth to house PMs in slots and avoid potential movement. Benefiting from the concentrated winding connection, the wiring process is simplified, and the winding ends are short. Fig. 25(c) shows the laminations of rotor core. The rotor core is connected to two end discs by screw for mechanical support. A test platform is built in Fig. 26, which consists of the prototype, dynamometer, drive controller, power source and oscilloscope.

Firstly, the no-load tests are performed. By injecting constant DC current into each sub-phase module, back EMF at 1000 rpm is measured and presented in Fig. 27. The tested result basically agrees with that from the FE prediction, while their difference mainly exists in third-order harmonic distribution, which is due to fabrication tolerance such as nonuniform PM magnetization. The cogging torque is measured by collecting the locked torque at different positions. As shown in Fig. 28, the measured result is relatively larger considering mechanical eccentricity.

Then, by using zero-sequence current control, integrated AC and DC current are injected into armature terminal, as shown in Fig. 29. The DC current ratio is set at 0.5 for maximum torque generation. The steady torque value at different electrical load is plotted in Fig. 30. It is shown, compared to the design without slot PMs, torque capacity of RDCS-HVM is enhanced by 12% with 12A/mm^2 current density and 25% with 24A/mm^2 current density. The prototype specifications at rated condition as well as simulation data, are all listed in Table V.

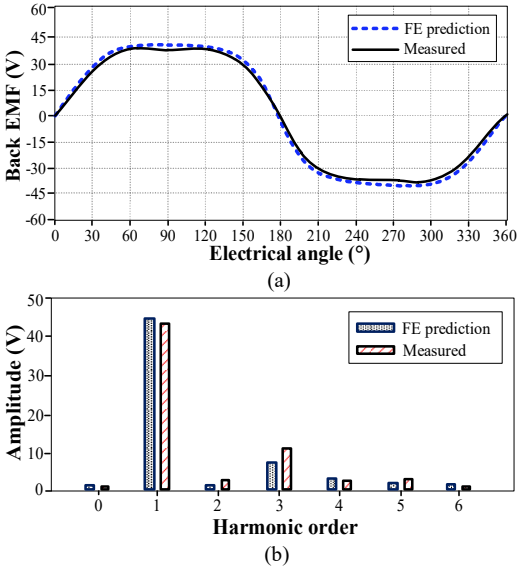

Fig. 27. (a) Back EMF at 1000 rpm with 6A DC current. (b) FFT analysis.

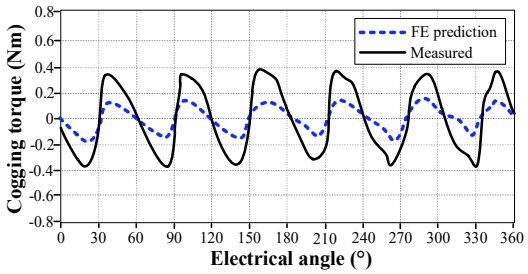

Fig. 28. Cogging torque with 6A DC current.

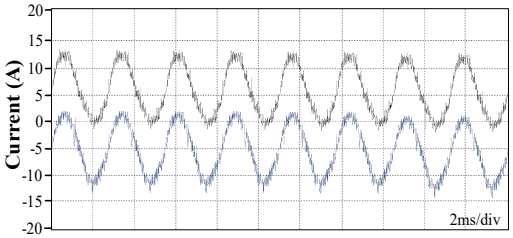

Fig. 29. Integrated current excitation in two sub-phases of phase A.

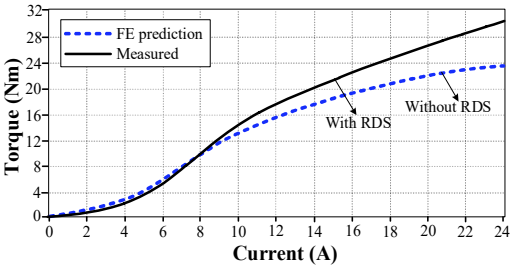

Fig. 30. Torque ability under different electrical load.

Finally, the electromagnetic performance at fault conditions is evaluated. Due to the special PM arrangement, the change of PM working point is not significant. Therefore, the open-circuit voltage is small as shown Fig. 31(a). By directly connecting the winding terminals, the short-circuit current at different speeds is collected in Fig. 31(b), which is far less than the rated current. The torque performance at normal, fault and active fault control conditions are measured and plotted in Fig. 32. In general, good fault-tolerant performance is achieved in this new topology.

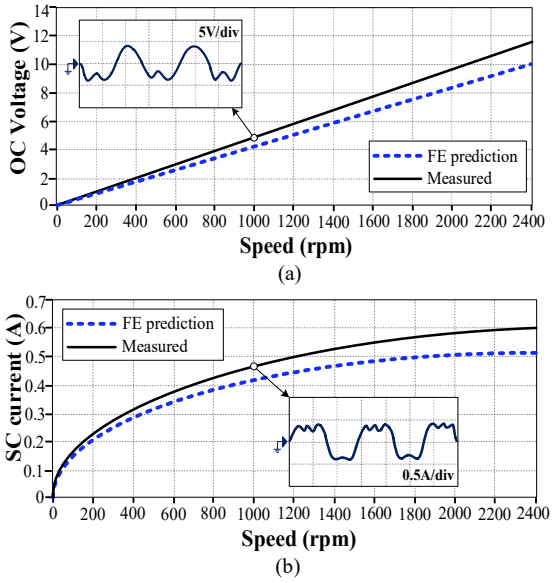

Fig. 31. (a) Open-circuit voltage. (b) Short-circuit current.

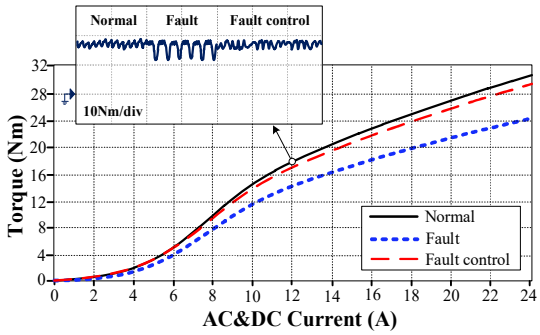

Fig. 32. Torque at normal, fault and fault-tolerant status.

VII. Conclusion

This paper proposes a new relieving-DC-saturation hybrid reluctance machine for fault-tolerant in-wheel direct drive. This machine utilizes the zero-sequence current to replace extra DC field coils for efficient torque generation. Further, slot PMs are artificially introduced to mitigate the intrinsic DC saturation in stator core and thus enhance core utilization and torque density. Moreover, with modular magnetic field, the proposed machine exhibits excellent fault-tolerant ability at both open-circuit and short-circuit conditions. Finite element analysis and prototype tests demonstrate the feasibility of the proposed topology. Some design guidelines for this new topology are provided as

(1) The slot pole combination has a leading influence on torque performance. To mitigate the torque ripple caused by reluctance torque and cogging torque, the 24-slot and 22-pole-pair design is recommended due to its electromagnetic complementation.

(2) The slot PM dosage should be accurately designed to obtain a balance between the relieving-DC-saturation effect, electrical load reduction and machine cost increase.

(3) The DC current ratio should be equal to or larger than 0.5 to achieve both acceptable torque density and power factor.

(4) The slot PMs do not contribute to torque generation directly, and thus the PM utilization is lower than that in traditional PM machines. In future work, using ferrite magnets to replace rare-earth PMs can help to relieve PM utilization and cost issue.

References

[1] A. Emadi, Y. J. Lee, and K. Rajashekara, "Power electronics and motor drives in electric, hybrid electric, plug-in hybrid electric vehicles," *IEEE Trans. Ind. Electron.*, vol. 55, no. 6, pp. 2237–2245, Jun. 2008.

[2] L. De Novellis, A. Sorniotti, and P. Gruber, "Wheel torque distribution criteria for electric vehicles with torque-vectoring differentials," *IEEE Trans. Veh. Technol.*, vol. 63, no. 4, pp. 1593–1602, May 2014.

[3] A. M. Dizqah, and J. De Smet "A fast and parametric torque distribution strategy for four-wheel-drive energy-efficient electric vehicles," *IEEE Trans. Ind. Electron.,* vol. 63, no. 7, pp. 4367–4376, Jul. 2016.

[4] S. U. Chung, S. H. Moon, and D. J. Kim, "Development of a 20-Pole-24-Slot SPMSM with consequent pole rotor for in-wheel direct drive," *IEEE Trans. Ind. Electron.*, vol. 63, no. 1, pp. 302-309, Jan. 2016.

[5] Y. Du, W. Lu, X. Zhu and L. Quan, "Optimal design and analysis of partitioned stator hybrid excitation doubly salient machine," *IEEE Access*, vol. 6, pp. 57700-57707, 2018.

[6] X. Zhao and S. Niu, "Design and optimization of a novel slot-PM-assisted variable flux reluctance generator for hybrid electric vehicles," *IEEE Trans. Energy Convers*., vol. 33, no. 4, pp. 2102-2111, Dec. 2018.

[7] X. D. Xue, and N. C. Cheung, "Multi-objective optimization design of in-wheel switched reluctance motors in electric vehicles," *IEEE Trans. Ind. Electron.*, vol. 57, no. 9, pp. 2980-2987, Sept. 2010.

[8] J. Zhu, K. W. E. Cheng, and X. Xue, "Design of a new enhanced torque in-Wheel switched reluctance motor with divided teeth for electric vehicles," *IEEE Trans. Magn.*, vol. 53, no. 11, pp. 1-4, Nov. 2017.

[9] P. Andrada, B. Blanqué, E. Martínez, M. Torrent, "A novel type of hybrid reluctance motor drive", *IEEE Trans. Ind. Electron.*, vol. 61, no. 8, pp. 4337-4345, Aug. 2014.

[10] J. Zhu, K. W. E. Cheng and X. Xue, "Design and analysis of a new enhanced torque hybrid switched reluctance motor," *IEEE Trans. Energy Convers*, vol. 33, no. 4, pp. 1965-1977, Dec. 2018.

[11] S. Ullah, S. P. McDonald, R. Martin, M. Benarous and G. J. Atkinson, "A permanent magnet assist, segmented rotor, switched reluctance drive for fault tolerant aerospace applications," *IEEE Trans on Indus. Appl.*, vol. 55, no. 1, pp. 298-305, Jan.-Feb. 2019.

[12] X. Deng, B. Mecrow, H. Wu and R. Martin, "Design and development of low torque ripple variable-speed drive system with six-phase switched reluctance motors," *IEEE Trans. Energy Convers*., vol. 33, no. 1, pp. 420-429, March 2018.

[13] Y. Jin, B. Bilgin, and A. Emadi, "An extended-speed low-ripple torque control of switched reluctance motor drives," *IEEE Transactions on Power Electronics*, vol. 30, pp. 1457-1470, 2015

[14] Y. Wang, and Z. Zhang, "Torque density improvement of doubly salient electromagnetic machine with asymmetric current Control," *IEEE Trans. Ind. Electron.*, vol. 63, no. 12, pp. 7434-7443, Dec. 2016.

[15] Z. Chen, and H. Wang, "A doubly salient starter/generator with two-section twisted-rotor structure for potential future aerospace application," *IEEE Trans. Ind. Electron.*, vol. 59, no. 9, pp. 3588-3595, Sept. 2012.

[16] X. Liu, Z. Q. Zhu, "Electromagnetic performance of novel variable flux reluctance machines with DC-field coil in stator", *IEEE Trans. Magn.*, vol. 49, no. 6, pp. 3020-3028, Jun. 2013.

[17] X. Liu and Z. Q. Zhu, "Stator rotor pole combinations and winding configurations of variable flux reluctance machines," *IEEE Trans. Ind. Appl*, vol. 50, no. 6, pp. 3675-3684, Nov.-Dec. 2014.

[18] X. Liu, Z. Q. Zhu, "Comparative study of novel variable flux reluctance machines with doubly fed doubly salient machines", *IEEE Trans. Magn.*, vol. 49, no. 7, pp. 3838-3841, Jul. 2013.

[19] Z. Q. Zhu and B. Lee, "Integrated field and armature current control for dual three-phase variable flux reluctance machine drives," *IEEE Trans on Energy Convers.,* vol. 32, no. 2, pp. 447-457, June 2017.

[20] S. Jia, and R. Qu, "Hybrid excitation stator PM Vernier machines with novel DC-biased sinusoidal armature current," *IEEE Trans. Ind. Appl*, vol. 54, no. 2, pp. 1339-1348, March-April 2018.

[21] Q. Wang, S. Niu and X. Luo, "A novel hybrid dual-PM machine excited by AC with DC bias for electric vehicle propulsion," *IEEE Trans. Ind. Electron.*, vol. 64, no. 9, pp. 6908-6919, Sept. 2017.

[22] X. Zhao, and S. Niu, "A new modular relieving-DC-saturation Vernier reluctance machine excited by zero-sequence current for electric vehicle," *IEEE Trans. Magn*, vol. 55, no. 7, pp. 1-5, July 2019

[23] S. Xue, J. Feng, S. Guo and Z. Q. Zhu *et al*, "Iron loss model under DC bias flux density considering temperature influence," *IEEE Trans. Magn.*, vol. 53, no. 11, pp. 1-4, Nov. 2017.

Xing Zhao received the B.Sc. degree in Electrical Engineering from the department of Automation at Nanjing University of Aero & Astro, China, in 2014, and currently he is pursuing Ph.D. degree in Electrical Engineering at the department of Electrical Engineering at the Hong Kong Polytechnic University, Hong Kong. His research interests involve new electrical machines and drives for electric vehicles and renewable power generation.

Shuangxia Niu received the B.Sc. and M.Sc. degrees from Tianjin University, China, in 2002 and 2005, respectively, and the Ph.D. degree from the University of Hong Kong, Hong Kong, in 2009, all in electrical engineering. Currently she is an Associate Professor in the Department of Electrical Engineering at Hong Kong Polytechnic University, Hong Kong. She has authored or coauthored over 100 papers in leading journals. Her research interests are electrical machines and drives for electric vehicles, renewable energy conversion, and applied electromagnetics.

Xiaodong Zhang received the B.Eng. and M.Eng. degrees in Electrical Engineering from the Department of Automation, Tianjin University, China, in 2002 and 2005, respectively. He received the Ph.D. degree in electrical engineering from the Department of Electrical and Electronic Engineering, the University of Hong Kong, Hong Kong, in 2011. His research interests include design and control of electric machines for electric vehicles.

W.N. Fu received the B.Eng. degree from Hefei University of Technology, Hefei China, in 1982, the M.Eng. degree from Shanghai University of Technology, Shanghai, China, in 1989, and the Ph.D. degree from Hong Kong Polytechnic University, Hong Kong, in 1999, all in electrical engineering. He is currently a Professor at Hong Kong Polytechnic University. Before joining the university in 2007, he was one of the Key Developers at Ansoft Corporation, Pittsburgh, PA, USA. He has about seven years of working experience at Ansoft, focusing on the development of the commercial software Maxwell. His current research interests include electromagnetic field computation, applied electromagnetics, and novel electric machines.